HHS Public Access

Author manuscript

ACS Biomater Sci Eng. Author manuscript; available in PMC 2016 December 07.

Published in final edited form as:

ACS Biomater Sci Eng. 2016 October 10; 2(10): 1806–1816. doi:10.1021/acsbiomaterials.6b00101.

Three-Dimensional Printing of Bone Extracellular Matrix for Craniofacial Regeneration

Ben P. Hung[†,‡], **Bilal A. Naved**[‖], **Ethan L. Nyberg**[†,‡], **Miguel Dias**[†,‡], **Christina A. Holmes**[§], **Jennifer H. Elisseeff**[†,‡], **Amir H. Dorafshar**[*,⊥], and **Warren L. Grayson**[*,†,‡]

[†]Department of Biomedical Engineering, The Johns Hopkins University School of Medicine, Baltimore 21231, Maryland, United States

[‡]Translational Tissue Engineering Center, The Johns Hopkins University School of Medicine, Baltimore 21231, Maryland, United States

[§]Department of Neurosurgery, The Johns Hopkins Hospital, Baltimore 21231, Maryland, United States

[⊥]Department of Plastic Surgery, The Johns Hopkins Hospital, Baltimore 21231, Maryland, United States

[‖]Fischell Department of Biomedical Engineering, University of Maryland, College Park, Maryland 21231, United States

Abstract

Tissue-engineered approaches to regenerate bone in the craniomaxillofacial region utilize biomaterial scaffolds to provide structural and biological cues to stem cells to stimulate osteogenic differentiation. Bioactive scaffolds are typically comprised of natural components but often lack the manufacturability of synthetic materials. To circumvent this trade-off, we 3D printed materials comprised of decellularized bone (DCB) matrix particles combined with polycaprolactone (PCL) to create novel hybrid DCB:PCL scaffolds for bone regeneration. Hybrid scaffolds were readily printable at compositions of up to 70% bone by mass and displayed robust mechanical properties. Assessments of surface features revealed both collagenous and mineral components of bone were present. Qualitative and quantitative assessments showed increased surface roughness relative to that of pure PCL scaffolds. These findings correlated with enhanced cell adhesion on hybrid surfaces relative to that on pure surfaces. Human adipose-derived stem cells (hASCs) cultured in DCB:PCL scaffolds without soluble osteogenic cues exhibited significant upregulation of osteogenic genes in hybrid scaffolds relative to pure PCL scaffolds. In the presence of soluble phosphate, hybrid scaffolds resulted in increased calcification. The hASC-seeded scaffolds were implanted into critical-sized murine calvarial defects and yielded greater bone regeneration in

[*]**Corresponding Authors:** 601 N. Caroline Street, Baltimore, MD 21231; adorafs1@jhmi.edu.; 400 N. Broadway, Smith 5023, Baltimore, MD 21231; tel: 410-502-6306; fax: 410-502-6308; wgrayson@jhmi.edu.

Supporting Information

The Supporting Information is available free of charge on the ACS Publications website at DOI: 10.1021/acsbiomaterials.6b00101. (Figure S1) Scanning electron microscopy images of cryo-milled bone particles and (Figure S2) infiltration of endogenous cells into scaffolds following 1 week implantation in murine calvarial defect (PDF)

Notes

The authors declare no competing financial interest.

DCB:PCL scaffolds compared to that in PCL-only at 1 and 3 months post-transplantation. Taken together, these results demonstrate that 3D printed DCB:PCL scaffolds might be effective for stimulating bone regeneration.

Graphical abstract

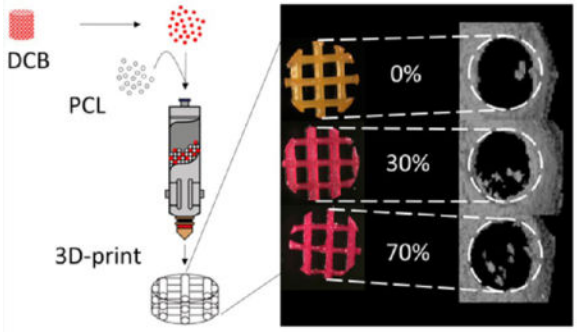

Keywords

tissue engineering; bone regeneration; 3D-printing; biomaterials; decellularized bone

INTRODUCTION

Craniomaxillofacial (CMF) injuries, resulting from congenital defects,[1] trauma,[2] and surgical resection,[3] are a significant clinical challenge. CMF injuries negatively impact patient speaking ability, eating behaviors, and psychosocial well-being. Approximately 200,000 CMF injuries occur annually, incurring a significant economic burden.[4]

The current gold standard for CMF repair is the autologous vascularized free fibular flap;[5,6] however, this technique relies on a limited source of donor tissue and incurs donor-site morbidity. In addition, the complex geometries of bone within the CMF region cannot be easily recapitulated using fibular segments. Although prosthetic implants have been investigated, no single method presents an ideal solution.[7] The widely used poly[methyl methacrylate] implant has disadvantages in its highly exothermic synthesis, which can lead to tissue necrosis in the CMF region as well as its brittle mechanical properties.[8] Another widely used material, titanium, has superior mechanical properties, but has high costs and low hard-tissue integration with native bone;[9] furthermore, it carries risks of soft tissue dehiscence and inflammation. Finally, the use of prosthetic implants in younger patients, whose tissue continues to grow, remains a challenge as multiple revision surgeries are needed to accommodate the growing tissue. Tissue engineering of bone presents a possible solution to these drawbacks. Traditionally, bone progenitor cells are combined with a biomaterial scaffold and signaled with appropriate bioactive factors to create a construct that will regenerate lost tissue.[10] The ideal tissue engineering approach to repairing CMF defects would result in a completely biological tissue that is capable of adapting to physiological cues, overcoming the limitation of prosthetics. Although bone engineering approaches have enjoyed several advancements, the choice of the scaffold is still associated with several

challenges. For CMF bone, this biomaterial scaffold is critical, as it determines mechanical properties and tissue geometry.

Current materials used to engineer scaffolds fall into two general categories: naturally derived and synthetic. Although several naturally derived materials have been used in bone engineering, such as collagen sponges[11] and chitosan,[12] the gold standard for bone scaffolds within tissue engineering is allogenic decellularized trabecular bone (DCB), notable for its intrinsic osteoinductivity, osteoconductivity, and appropriate mechanical properties.[13–16] As a result, DCB scaffolds have been widely used in bone engineering investigations.[17–21] Our group has previously produced DCB scaffolds in the shape of the temporomandibular joint condyle, demonstrating the potential for these scaffolds in recapitulating complex CMF geometries.[22] Despite recapitulating the appropriate anatomic geometry, obtaining clinically relevant and continuous volumes of trabecular bone for scaffold production is challenging. To overcome these limitations, synthetic scaffolds have been produced using various biomaterials, such as poly[lactic acid] and poly[glycolic acid].[23] Notably, synthetic scaffolds can harness the capabilities of fabrication via three-dimensional printing,[24,25] a particular advantage for bone engineering in the CMF region due to the complex geometries in this region. Our group has fabricated polycaprolactone (PCL) scaffolds in the shape of the mandible and maxilla via 3D-printing, demonstrating the potential of this technology for producing CMF geometries of a size scale above that possible using DCB scaffolds.[26] In particular, the relatively low melting point of PCL, 60 °C, makes it well-suited to extrusion-based 3D-printing. Although this approach is promising, synthetic scaffolds lack the osteoinductivity and osteoconductivity of naturally derived scaffolds.

Functionalizing synthetic scaffolds to impart bioactivity, such as by incorporating appropriate osteoinductive growth factors[27] or incorporation of mineral phases,[28–31] has had some success in overcoming this challenge; however, these approaches do not recapitulate the full bioactivity of DCB scaffolds. Namely, they do not include the collagenous phase of bone, which has been shown to enhance osteogenesis in dogs when combined with tricalcium phosphate implants compared to that with tricalcium phosphate alone.[32] Our previous studies using collagen in conjunction with bone scaffolds resulted in increased cell migration throughout the scaffold.[21] In this study, we hypothesized that, by incorporating DCB particles into PCL, we could create a hybrid DCB:PCL material that incorporates both mineral and collagenous bioactive phases of bone, maintains the osteoinductive and osteoconductive properties of DCB, and is readily manufactured by 3D printing. The objectives of this study were to (1) evaluate print quality of 3D-printed hybrid scaffolds at different DCB:PCL ratios, (2) determine the mechanical properties of hybrid scaffolds, (3) characterize the ability of human adipose-derived stem cells (hASCs, a cell type used successfully in bone engineering applications) to adhere to the DCB:PCL hybrid material, (4) assess the ability of DCB:PCL scaffolds to differentiate resident hASCs to bone, and (5) assess the ability of the DCB:PCL material to regenerate bone in an orthotopic cranial defect.

EXPERIMENTAL SECTION

Creation of Hybrid Material

Trabecular bone was obtained from the subchondral region of 0.5–4 month old calves. Decellularization proceeded as previously described.[21,33] Bone was first subjected to a high-pressure water jet to wash out the marrow. Then, bones were washed with phosphate-buffered saline (PBS; Cellgro, Manassas, VA) containing 0.1% w/v ethylenediaminetetraacetic acid (EDTA; Sigma-Aldrich, St. Louis, MO) for 1 h at room temperature and then overnight with PBS containing 0.1% w/v EDTA and 10 mM Tris (Sigma-Aldrich) at 4 °C. Bones were then washed for another hour in PBS before being subjected to a wash consisting of PBS with 10 mM Tris and 0.5% sodium dodecyl sulfate (SDS; Sigma-Aldrich) for 1 day at room temperature. The SDS was removed with extensive PBS washes and then the bones were washed with PBS containing 10 mM Tris, 50 U/mL DNase (Roche Applied Science, Indianapolis, IN), and 1 U/mL RNase (Roche Applied Science) for 5 h at room temperature. Enzymes were removed with extensive PBS and water washes before storage via lyophilization.

Decellularized trabecular bone was pulverized using a SPEX SamplePrep 6770 cryo-mill (SPEX SamplePrep, Metuchen, NJ) at a frequency of 10 Hz for 15 min to obtain bone particles. The particles were then run through a 40 μm cell strainer to confine maximum particle size to 40 μm, a step performed to minimize risk of particle aggregation and clogging of the printer nozzle. This size of particles was confirmed via scanning electron microscopy (SEM; Figure S1). The resulting bone particles were mixed with PCL powder with molar mass of 43000–50000 g/mol (Polysciences Incorporated, Warrington, PA) for printing.

Scaffold Fabrication and Evaluation of Print Quality

Hybrid mixtures consisting of 0, 5, 30, 70, and 85% bone by mass were created and printed at 80 °C into 0.644 mm height (2 layer), 4 mm diameter scaffolds of 60% porosity using our custom 3D printer.[26] These parameters resulted in strut diameters of 460 μm and pore sizes were approximately 800 μm. This geometry was chosen to be consistent with the geometry required for the in vivo studies outlined below. Scaffold pore size was selected due to optimizations performed in a previous study in which 60% porosity was shown to yield the most uniform cell distribution during seeding.[26] Scaffolds were stained with Alizarin Red S (Sigma-Aldrich) to confirm the presence of mineralized particles and imaged under brightfield and scanning electron microscopy. Low-magnification brightfield images of scaffolds were compared pixel-by-pixel to a computer-generated ideal lattice. The percentage of pixels that matched between the two images was normalized to 50% to account for random matching, and this numerical score, ranging from 0 to 100, was taken as a measure of print quality.

Raman Spectroscopy

For determining the molecular constituents of the hybrid material and confirming the presence of both the mineral and collagen phases of the DCB particles, Raman spectroscopy was utilized as previously described.[34] Briefly, an 830 nm laser (Process Instruments, Salt

Lake City, UT) was used to deliver light to a sheet consisting of 30% bone by mass. Background subtraction and normalization was performed using a barium sulfate spectrum, and wavenumber assignment was performed using a Tylenol spectrum. As controls, the spectra of pure PCL and a block of decellularized trabecular bone were also obtained.

Atomic Force Microscopy

To determine the surface roughness of the hybrid material, atomic force microscopy (AFM) was performed on printed sheets of 0, 30, and 70% bone by mass using a Dimension 3100 AFM (Bruker Nano, Santa Barbara, CA) in tapping mode with Bruker Nano probe model RTESPW. The root-mean-square roughness of nine 2 μm × 2 μm square regions on each sample surface was measured at 15 Hz and averaged to determine the roughness of that sample. A total of three sample surfaces were tested for each DCB concentration.

Mechanical Testing

Solid cubes of 0, 30, and 70% bone by mass, 1.25 cm on all sides, were printed and subjected to unconfined compression using an EnduraTEC ELF 3200 system (Bose Corporation, Framingham, MA). As the specimens were solid, mechanical properties were assumed to be isotropic, and compression of up to 5% static strain was applied along the print axis, termed the *z*-axis, to determine the compressive modulus of the bulk material. Resulting expansion along the perpendicular *x*-axis was also measured to determine the Poisson's ratio. Three blocks for each DCB concentration were tested.

For measuring scaffold properties, porous cubes of 60% porosity and 1.25 cm on all sides were also printed. Because of the print layers, the properties along the *z*-axis differ from those of the other two axes; thus, the mechanical properties were assumed to be transversely isotropic. As such, compressive moduli were measured in both the *z*- and *x*-directions. Shear moduli were also measured with respect to the *x*-face along the *z*-direction. Three porous cubes for each DCB concentration were tested.

Measurement of Cell Adhesion Strength

As a measure of cell interaction with the hybrid material, the strength of cell adhesion to the hybrid material was quantified by a modification of a centrifugation assay described previously.[35,36] Briefly, fluorescently labeled cells were allowed to adhere to printed sheets of 0, 30, and 70% bone by mass for 24 h. Sheets were affixed onto a glass microscope slide using cyanoacrylate glue with the cells facing away from the slide. Slides were then immersed in PBS and subjected to centrifugation at different speeds. The position of the sheet on the slide relative to the centrifuge rotor as well as the centrifugation speed determined the shear stress applied to the cells[35]

$$\sigma = \|\vec{\omega}\|^2 y r_r (\Delta\rho) \quad (1)$$

where σ is the shear stress, $\vec{\omega}$ is angular velocity of the centrifuge where double bars denote vector magnitude, y is the average height of adhered cells as determined by microscopy, r_r is the distance from the rotor of the centrifuge, and $\Delta\rho$ is the difference in density between a

cell and the surrounding PBS. The fraction of remaining cells after each spin was plotted against the shear stress applied during that spin, and these data were fit to a variable-slope concentration response model (VSCR; eq 2[35,37,38]) to obtain a value for σ_{50}, the shear required for 50% of the cells on the sheet to detach

$$f = \frac{\sigma^a}{\sigma^a + \sigma_{50}^a} \quad (2)$$

where f is the fraction of cells adhered and a is a cooperativity coefficient of detachment. Four sheets composed of each DCB concentration were tested and the four values of σ_{50} were averaged for each material composition.

Measurement of Osteoinductivity

For measuring the ability of hybrid scaffolds to induce resident cells to undergo osteogenesis, hASCs of passage 2 were seeded into fibrin gels at 20 million cells per milliliter, and 5 μL gels were implanted into scaffolds of 0, 30, and 70% DCB by mass. Seeding proceeded as previously described[39] with a fibrinogen concentration of 10 mg/mL, thrombin concentration of 10 U/mL, and volume ratio of 4:1 fibrinogen/thrombin for a final fibrinogen concentration of 8 mg/mL and a final thrombin concentration of 2 U/mL. Scaffolds were 0.644 mm in height, 4 mm in diameter, and had 60% porosity. Scaffolds were sterilized by ethanol wash for 1 h at room temperature. hASCs were obtained as described previously.[39–41] All lipoaspirates obtained to isolate hASCs were obtained under Institutional Review Board approved protocols with patient consent. Briefly, lipoaspirate was digested with 1 mg/mL of collagenase I (Worthington Biochemical Corporation, Lakewood, NJ) for 1 h at 37 °C. The released cells were centrifuged to obtain the stromal vascular fraction pellet and plated. Adherent cells were termed hASCs and expanded for the current study. Expansion conditions consisted of Dulbecco's modified Eagle medium (DMEM; Life Technologies, Frederick, MD) with 4.5 g/L of glucose, 10% v/v fetal bovine serum (FBS; Atlanta Biologicals, Flowery Branch, GA), 100 U/mL of penicillin, 100 μg/mL of streptomycin (Cellgro), and 1 ng/mL of basic fibroblast growth factor (PeproTech, Rocky Hill, NJ). The hASCs from a single donor were used for all experiments in this study.

After seeding into scaffolds of 0, 30, and 70% DCB by mass, constructs were cultured for 1 and 3 weeks under control conditions: DMEM with 1 g/L of glucose, 100 U/mL of penicillin, 100 μg/mL of streptomycin, and 6% v/v FBS. The absence of osteoinductive factors ensured that only the scaffold could induce osteogenesis within resident cells. The sample size was $n = 3$ for each DCB concentration at each time point. After the culture periods, cells were digested with TRIzol (Life Technologies), and isolated mRNA was used to produce cDNA. cDNA was subject to real-time polymerase chain reaction (RT-PCR) for the osteogenic genes Runx2, osteocalcin (OCN), and osteonectin (ON) as previously described.[39] For analysis, the delta–delta Ct method was used in which β-actin served as the housekeeping gene and gene expression under pure PCL scaffolds served as the control group.

As an additional measure of osteoinductivity, constructs were also cultured for 3 weeks under osteogenic conditions, which consisted of control conditions supplemented with 10 mM β-glycerophosphate (Sigma-Aldrich) and 50 μM ascorbic acid (Sigma-Aldrich). These constructs were subject to the Quant-It PicoGreen dsDNA assay (Invitrogen, Carlsbad, CA) and the Stanbio LiquiColor calcium assay (Stanbio, Boerne, TX) to determine calcium content normalized to cell number as previously described.[39]

In Vivo Assessment of Bone Regeneration

For determining the effect of the hybrid scaffolds in vivo, the critically sized murine calvarial defect model was used as previously described.[39,42,43] All procedures were reviewed and approved by the Johns Hopkins Animal Care and Use Committee. Briefly, a 4 mm circular knife (Medicon, Tuttiligen, Germany) was used to excise a 4 mm disk of calvaria between the coronal and lambdoid sutures 1 mm lateral to the sagittal suture with care taken to preserve the underlying dura mater. This size has been shown previously by our group and others to be nonhealing.[39,42,43] Constructs consisting of hASCs seeded in fibrin inside scaffolds of 0, 30, and 70% bone by mass created as in the previous section were immediately implanted into the resulting defect. A total of 12 mice were operated on with n = 4 for each concentration of bone. The contralateral side served as unoperated controls. Mice were imaged under computed tomography (CT) using a Gamma Medica X-SPECT small animal system (Gamma Medica, Salem, NH) at 6 and 12 weeks postimplantation. Imaging was performed at 80 kV peak voltage and 600 μA current. Reconstruction was done with a voxel size of 100 μm. At 12 weeks postimplantation, scaffolds were excised and fixed under 3.7% formalin overnight for histological analysis as previously described.[39] Histological analysis consisted of a hematoxylin and eosin (H&E) stain for cellularity (Sigma-Aldrich) and a von Kossa and van Gieson stain for bone formation (Sigma-Aldrich).

RESULTS

Print Quality

DCB:PCL scaffolds of 0, 5, 30, 70, and 85% bone by mass were printed and stained with Alizarin Red S. We observed staining in all scaffolds except in the 0% scaffold, where no mineral was present, confirming the presence of bone particles within the hybrid scaffolds. The intensity of the red stain increased with increasing DCB concentration (Figure 1). When compared to a computer-generated ideal lattice, the print quality decreased as the concentration of bone increased from a score of roughly 89 for 0% and 5% DCB scaffolds to 77.6 for 70% DCB scaffolds; however, a dramatic drop in score (50) was observed at 85% DCB (Table 1). As such, for all subsequent studies, 70% bone by mass was chosen as the maximum concentration of bone; 0% bone by mass was chosen as a pure PCL control, and 30% bone by mass was chosen as an intermediate group.

Raman Spectroscopy

To confirm whether mineral and collagen were present on the surfaces of 3D-printed DCB:PCL, we employed Raman spectroscopy (Figure 2). Raman spectroscopy of a printed sheet of 30% bone by mass showed a peak at 960 cm^{-1} corresponding to the phosphate component of bone and a peak at 1650 cm^{-1} corresponding to the amide I signal from

collagen.[44] These peaks appear in the Raman spectrum of trabecular bone but not in the spectrum for pure PCL (Figure 2), matching observations reported previously.[45] The contributions from the PCL phase include the triple peak centered around 1450 cm^{-1} for δCH_2 (fourth carbon from the carbonyl), the double peak at 1300 cm^{-1} for ωCH_2 (furthest carbon from the carbonyl), and the skeletal stretching peak at 1110 cm^{-1},[45,46] which are signals appearing in the spectra for both pure PCL (Figure 2, top) and the 30% bone by mass sample (Figure 2, bottom).

Atomic Force Microscopy

SEM revealed that the surfaces of the 30 and 70% scaffolds displayed more features than those of the 0% scaffolds, whose surfaces were mostly smooth (Figure 1). For quantifying the surface roughness of scaffolds, which is known to affect cell–biomaterial interactions,[47–49] AFM was performed, and the root-mean-square roughness of 0, 30, and 70% scaffolds were computed. At the length scale of AFM, we found no significant difference between 30 and 70% scaffolds: both had roughness values around 50 nm. Both 30 and 70% scaffolds were significantly rougher than were 0% scaffolds, which showed a surface roughness of 4.83 nm (Figure 3), confirming observations under scanning electron microscopy.

Mechanical Properties

To determine how the bone particles affected the mechanical properties of the hybrid material, we first tested the compressive properties of the bulk material. The 0 and 30% blocks had similar compressive moduli of around 30 MPa, whereas the 70% blocks showed a significant drop in modulus to around 10 MPa. The Poisson's ratio of approximately 0.3 did not differ significantly between the three groups (Figure 4, top). The same trend held for the compressive and shear moduli of 60% porous scaffolds. The compressive modulus in the *x*-direction was similar for both the 0 and 30% scaffolds at around 15 MPa, whereas the modulus for 70% scaffolds was around 7 MPa. In the *z*-direction, 0 and 30% scaffolds had moduli approaching 10 MPa, whereas the 70% scaffolds had moduli approaching 5 MPa (Figure 4, bottom).

Cell–Biomaterial Adhesion

We next characterized cell adhesion to the hybrid material as an indicator of cell–material interactions. The centrifuge-applied shear successfully detached cells in a force-dependent manner, and the VSCR model[35,37,38] fit the data well (Figure 5, top). The shear for half-detachment, σ_{50}, was significantly different between all three groups (Figure 5, bottom), increasing in a concentration-dependent manner from 0.0872 Pa for pure PCL adhesion to 28.2 Pa for adhesion to 70% bone by mass. This observation is well-supported by the surface biomolecular data (Figure 2) and the surface roughness data (Figures 1 and 3).

As an in vivo correlation that the observed concentration-dependent trend occurs with cell invasion, acellular scaffolds were implanted in the murine calvarial defect and excised for H&E after 1 week. Although little cell invasion was observed in 0% scaffolds, a concentration-dependent increase in cell invasion occurred with increasing concentration of bone in hybrid scaffolds (Figure S2). Taken together, this data confirms that hybrid scaffolds

are more amenable to cell adhesion and migration when compared to those of pure PCL scaffolds.

In Vitro Osteoinductivity

Because the goal of this study was to enhance bone regeneration, we next examined the ability of hybrid scaffolds to induce resident cells to form bone. By 3 weeks of culture, Runx2 expression increased by more than 3 orders of magnitude whereas OCN and ON expression increased by approximately 5 orders of magnitude compared to PCL alone despite the absence of soluble osteoinductive factors in the culture medium (Figure 6). Because no phosphate source was present, this increase in gene expression did not yield calcium production; however, when a phosphate source was added with ascorbic acid and constructs cultured for 3 weeks, the hybrid scaffolds displayed higher calcium production per cell relative to pure PCL controls with 70% scaffolds yielding 88.0 ng/cell and 30% scaffolds yielding 48.1 ng/cell compared to 35.3 ng/cell from pure PCL scaffolds (Figure 6). Because little to no calcium was detected in samples with no phosphate, it can be surmised that the calcium content innately present in the hybrid scaffold was not being detected by the assay.

In Vivo Osteoinductivity

As a final assessment of the osteoinductive properties of hybrid scaffolds relative to those of pure PCL scaffolds, scaffolds of 0, 30, and 70% bone by mass were fabricated and seeded with hASCs as was done in the in vitro experiment. The resulting constructs were implanted in 4 mm murine calvarial defects. CT scans at both 6 and 12 weeks postimplantation revealed that hybrid scaffolds invoked nearly twice the volume of regenerated bone compared to that from pure PCL scaffolds (Figure 7) with hybrid scaffolds approaching 4 mm^3 of regenerated bone compared to 2.07 mm^3 regenerated bone with pure PCL scaffolds. The pattern of signal detected by CT within the defect suggested that the system was not picking up the mineral innately present within the hybrid scaffolds, as the detected bone was punctate and isolated rather than ubiquitously present within the scaffold struts (which were not visible under CT). CT scans also revealed that regenerated bone appeared in both the scaffold centers as well as from the edges, suggesting that implanted cells within the scaffold and invading cells from the host were both contributing to repair. Histological analysis (Figure 8) revealed the presence of both nonmineralized osteoid and mineralized tissue, as visualized by the van Gieson and von Kossa stains, respectively, indicating that bone regeneration was actively occurring within the defect.

3D Printing of Anatomical Geometry

For demonstrating the ability of the approach described here to create anatomical shapes, the geometry of the human temporomandibular joint condyle was extracted and printed using pure PCL as well as 30% bone by mass. The scaffolds printed successfully and were subject to Alizarin Red S staining to confirm the presence of bone mineral (Figure 9). Although the pure PCL condyle did not stain, as expected, robust staining was observed in the 30% bone by mass condyle, demonstrating that 3D printing of hybrid material can be used to fabricate complex craniofacial geometries.

DISCUSSION

In this study, hybrid scaffolds consisting of bone particles embedded in a greater polycaprolactone phase were printed using a custom 3D printer. To our knowledge, this is the first time a bone engineering hybrid scaffold has been fabricated by 3D printing of naturally derived ECM. In addition to being readily printable, hybrid scaffolds are more amenable to cell adhesion compared to pure PCL scaffolds and are osteoinductive both in vitro and in vivo. As such, the hybrid material developed here mitigates the lack of osteoinductivity and osteoconductivity in pure PCL while simultaneously overcoming the manufacturing challenges associated with producing a pure decellularized trabecular bone scaffold.

We considered mechanics as a potential limiting factor in the use of this hybrid material, as mechanical properties for bone engineering scaffolds are crucial due to the role of bone as a load-bearing tissue. The choice of PCL as a biomaterial partly arises from this consideration, as its mechanical properties (stiffness on the order of 10^7 Pa) fall within the range reported for trabecular bone of 0.5–14.6 MPa.[50,51] Even with the drop in properties at 70% DCB by mass, the stiffness values reported for DCB:PCL scaffolds still approach the values of trabecular bone and are within the range reported in the literature for pure PCL 3D-printed scaffolds.[52,53] Composite collagen/calcium phosphate-printed scaffolds were reported to have a modulus of approximately 15 MPa, comparable to the values in the present study;[54] however, it should be noted that the porosity in the present study–an important property for highly osteoconductive scaffolds–is much greater in comparison while still retaining appropriate moduli. Taken together, this data suggests that mechanics is not a limiting factor in the use of these hybrid scaffolds in bone engineering.

Next, we examined the interactions between human stem cells and the hybrid material. We investigated two important aspects of cell–biomaterial interactions: cell adhesion to biomaterials has been studied extensively and affects many aspects of cell behavior, whereas cell migration through a biomaterial scaffold is crucial for a uniformly seeded graft as well as for recruitment of host cells to the implant. The SEM and AFM data on surface roughness indicated that this was a feature of the printed hybrid material that could enhance cell adhesion at different length scales–the micrometer scale as shown under SEM and the nanometer scale as shown under AFM. Meanwhile, the presence of collagen as confirmed by Raman spectroscopy suggested that an increased number of binding sites could be a second mode by which the hybrid material could enhance cell adhesion. The data demonstrates increasing cell adhesion strength with higher concentrations of bone in the scaffolds. In comparison, the shear forces required for half-detachment of ASCs seeded on scaffolds containing 70% bone by mass (~30 Pa) agrees well with previous studies on cell adhesion to hydroxyapatite.[55] Although it should be noted that the values reported here for initial cell numbers reflect a combination of initial adhesion and proliferation after 1 day, the trend that higher concentration of DCB leads to increased σ_{50}, an effect of surface roughness, the presence of collagen, or both, remains true.

The RT-PCR data are derived from ASCs grown in scaffolds in vitro and provide evidence that the hybrid scaffolds are innately osteoinductive. The RQ values reported are normalized

to expression in pure PCL scaffolds, where no osteoinductive cues were present and little expression of osteogenic genes is expected. Interestingly, the osteogenic gene expression in hybrid DCB:PCL scaffolds increased compared to that in pure PCL scaffolds despite the absence of soluble osteoinductive factors in the culture medium. The observation that calcium per cell in pure PCL scaffolds matches closely with previously reported values (30–40 ng/cell[39]) and increases in hybrid scaffolds demonstrates both the osteogenic capability of the cells as well as the ability of the hybrid scaffold to enhance this capability. The changes in bone volume following transplantation of ASC-seeded scaffolds into orthotopic defects also supported the hypothesis that hybrid scaffolds are osteoinductive compared to pure PCL scaffolds. Note that in that particular experiment, the cells were not provided any soluble osteoinductive cues prior to implantation. Consequently, differentiation cues were provided solely by the DCB:PCL hybrid scaffolds. The percent of bone regenerated in the current study is also comparable to previous studies where PCL:tricalcium phosphate:collagen scaffolds were implanted into rat calvariae.[56]

In examining the spatial profile of the bone formed, bone is visible both in the scaffold pore spaces and in the scaffold edges. As such, it is possible to speculate that two factors are at play: bone being regenerated from the implanted human cells, which are distributed throughout the scaffold and therefore can regenerate bone from the scaffold interior, as well as bone regenerated from endogenous murine cells as they migrate in from the scaffold periphery. Although it is outside the scope of this study to distinguish between these two sources of regeneration and their respective roles, future studies may examine this further. It is worth noting that the hybrid scaffold potentially enhances both of these avenues of regeneration due to both mineral and collagenous phases enhancing osteoinductivity and osteoconductivity.

Although we have demonstrated here a printable, bioactive scaffold, future optimizations may be performed. First, the particle size of DCB was chosen at a maximum of 40 μm in the current study to reduce the chance of particle aggregation blocking flow from the print nozzle, which has a diameter an order of magnitude above this size. In the current study, this particle size resulted in successful prints of bioactive scaffolds; however, it is possible that smaller particle sizes may further increase the amount of bone that can be printed as nozzle clogging becomes less of an issue. Another effect of particle size is the nanotopography of the scaffold, which we have shown here is affected at the nanoscale despite the microscale of the particles. Nanoscale changes in topography have been shown to affect the expression of osteocalcin in MSCs,[47] whereas the use of nanotopography to control cell shape was shown to modulate BMP-dependent osteogenesis.[57] Another effect of particle-mediated nanotopography is the potential for the particles to serve as nucleation sites for the deposition of mineral, leading to enhanced bone formation.[58] Taken together, this suggests that the DCB particle size alone may also play a role in enhancing the osteogenesis of seeded stem cells.

Second, the method of printing chosen here, an extrusion-based system, was selected due to its ease of use. Effectively, PCL was used as a “binder” to hold the DCB together. Other methods that have fabricated composite scaffolds, such as with synthetic ceramics, have used acidic binders that unfortunately result in decreased cell viability as well as smaller

pore size due to the increased flow of acidic binders away from the target print location.[54] It has been shown that smaller pore size inhibits the migration and proliferation of seeded and infiltrating cells.[59] As such, another advantage of the method used here is that PCL as the "binder" is readily printable, with minimal flow away from the target print location due to high viscosity, and is not cytotoxic. One potential shortcoming of this approach is the DCB is subject to 80 °C printing temperatures that destroy osteoinductive growth factors, such as BMP, that are known to reside in bone matrix;[13–15] however, many other methods of printing feature temperatures above this value, such as 1300 °C for sintering techniques.[60] Despite the elevated temperatures used in this study, the hybrid scaffolds produced in this study were still shown to be osteoinductive, likely due to the presence of the mineral phase; furthermore, the collagenous phase of bone was retained as shown by Raman spectroscopy. As such, the hybrid scaffold still represents an increase in bioactivity from pure PCL scaffolds while retaining printability. For the first time, bone matrix can be 3D-printed into any of the complex shapes in the human skeleton, representing a potentially storable, patient-specific component to tissue engineered bone grafts.

CONCLUSIONS

In this study, a hybrid material consisting of bone extracellular matrix embedded in a greater polycaprolactone phase was developed. This material is 3D printable while displaying osteoinductive properties in vitro and in vivo as evidenced by gene expression, calcium per cell, and in vivo bone regeneration of seeded human adipose-derived stem cells.

Supplementary Material

Refer to Web version on PubMed Central for supplementary material.

Acknowledgments

The authors thank Chi Zhang from Ishan Barman's laboratory at Johns Hopkins University for personal assistance in performing the Raman spectroscopy experiments, Professor Patricia McGuiggan at Johns Hopkins University for personal assistance in performing the atomic force microscopy experiments, and the Johns Hopkins School of Medicine Microscope Core Facility for aid in SEM use. The work was supported by NIH Ruth L. Kirschstein National Research Service Award grant F31 DE024922 and a Russell Military Scholar Award to B.P.H. and grants from the Department of Defense and Maryland Stem Cell Research Fund to W.L.G. A.H.D. thanks the American Maxillofacial Surgery Society Research Grant Award for support on this project.

References

1. Parker SE, Mai CT, Canfield MA, Rickard R, Wang Y, Meyer RE, Anderson P, Mason CA, Collins JS, Kirby RS, Correa A. Updated National Birth Prevalence estimates for selected birth defects in the United States, 2004–2006. Birth Defects Res, Part A. 2010; 88(12):1008–16.
2. Breeze J, Gibbons AJ, Shieff C, Banfield G, Bryant DG, Midwinter MJ. Combat-related craniofacial and cervical injuries: a 5-year review from the British military. J Trauma. 2011; 71(1):108–13. [PubMed: 21336187]
3. Wei FC, Seah CS, Tsai YC, Liu SJ, Tsai MS. Fibula osteoseptocutaneous flap for reconstruction of composite mandibular defects. Plast Reconstr Surg. 1994; 93(2):294–304. [PubMed: 8310021]
4. Desai BM. Osteobiologics. Am J Orthop. 2007; 36(4 Suppl):8–11.
5. Brydone AS, Meek D, Maclaine S. Bone grafting, orthopaedic biomaterials, and the clinical need for bone engineering. Proc Inst Mech Eng, Part H. 2011; 224(12):1329–43.

6. Broyles JM, Abt NB, Shridharani SM, Bojovic B, Rodriguez ED, Dorafshar AH. The fusion of craniofacial reconstruction and microsurgery: a functional and aesthetic approach. Plast Reconstr Surg. 2014; 134(4):760–9. [PubMed: 25357035]
7. Reddy S, Khalifian S, Flores JM, Bellamy J, Manson PN, Rodriguez ED, Dorafshar AH. Clinical outcomes in cranioplasty: risk factors and choice of reconstructive material. Plast Reconstr Surg. 2014; 133(4):864–73. [PubMed: 24675189]
8. Benzel EC, Thammavaram K, Kesterson L. The diagnosis of infections associated with acrylic cranioplasties. Neuroradiology. 1990; 32(2):151–3. [PubMed: 2398941]
9. Park HK, Dujovny M, Agner C, Diaz FG. Biomechanical properties of calvarium prosthesis. Neurol Res. 2001; 23(2–3):267–76. [PubMed: 11320607]
10. Langer R, Vacanti JP. Tissue engineering. Science. 1993; 260(5110):920–6. [PubMed: 8493529]
11. Iejima D, Saito T, Uemura T. A collagen-phosphophoryn sponge as a scaffold for bone tissue engineering. J Biomater Sci, Polym Ed. 2003; 14(10):1097–1103. [PubMed: 14661881]
12. Ucar S, Yilgor P, Hasirci V, Hasirci N. Chitosan-based wet-spun scaffolds for bioactive agent delivery. J Appl Polym Sci. 2013; 130(5):3759–3769.
13. Urist MR. Bone: formation by autoinduction. Science. 1965; 150(3698):893–9. [PubMed: 5319761]
14. Urist MR, Mikulski A, Lietze A. Solubilized and insolubilized bone morphogenetic protein. Proc Natl Acad Sci U S A. 1979; 76(4):1828–32. [PubMed: 221908]
15. Sampath TK, Reddi AH. Dissociative extraction and reconstitution of extracellular matrix components involved in local bone differentiation. Proc Natl Acad Sci U S A. 1981; 78(12):7599–603. [PubMed: 6950401]
16. Harakas NK. Demineralized bone-matrix-induced osteogenesis. Clin Orthop Relat Res. 1984; (188):239–51.
17. Mauney JR, Blumberg J, Pirun M, Volloch V, Vunjak-Novakovic G, Kaplan DL. Osteogenic differentiation of human bone marrow stromal cells on partially demineralized bone scaffolds in vitro. Tissue Eng. 2004; 10(1–2):81–92. [PubMed: 15009933]
18. Mauney JR, Jaquiery C, Volloch V, Heberer M, Martin I, Kaplan DL. In vitro and in vivo evaluation of differentially demineralized cancellous bone scaffolds combined with human bone marrow stromal cells for tissue engineering. Biomaterials. 2005; 26(16):3173–3185. [PubMed: 15603812]
19. Marcos-Campos I, Marolt D, Petridis P, Bhumiratana S, Schmidt D, Vunjak-Novakovic G. Bone scaffold architecture modulates the development of mineralized bone matrix by human embryonic stem cells. Biomaterials. 2012; 33(33):8329–42. [PubMed: 22901965]
20. Gerhardt LC, Widdows KL, Erol MM, Nandakumar A, Roqan IS, Ansari T, Boccaccini AR. Neocellularization and neovascularization of nanosized bioactive glass-coated decellularized trabecular bone scaffolds. J Biomed Mater Res, Part A. 2013; 101(3):827–41.
21. Hung BP, Salter EK, Temple J, Mundinger GS, Brown EN, Brazio P, Rodriguez ED, Grayson WL. Engineering bone grafts with enhanced bone marrow and native scaffolds. Cells Tissues Organs. 2013; 198(2):87–98. [PubMed: 24021248]
22. Grayson WL, Frohlich M, Yeager K, Bhumiratana S, Chan ME, Cannizzaro C, Wan LQ, Liu XS, Guo XE, Vunjak-Novakovic G. Engineering anatomically shaped human bone grafts. Proc Natl Acad Sci U S A. 2010; 107(8):3299–304. [PubMed: 19820164]
23. Saito E, Liao EE, Hu WW, Krebsbach PH, Hollister SJ. Effects of designed PLLA and 50:50 PLGA scaffold architectures on bone formation in vivo. J Tissue Eng Regener Med. 2013; 7(2): 99–111.
24. Eshraghi S, Das S. Mechanical and microstructural properties of polycaprolactone scaffolds with one-dimensional, two-dimensional, and three-dimensional orthogonally oriented porous architectures produced by selective laser sintering. Acta Biomater. 2010; 6(7):2467–76. [PubMed: 20144914]
25. Park SH, Park DS, Shin JW, Kang YG, Kim HK, Yoon TR. Scaffolds for bone tissue engineering fabricated from two different materials by the rapid prototyping technique: PCL versus PLGA. J Mater Sci: Mater Med. 2012; 23(11):2671–8. [PubMed: 22990617]

26. Temple JP, Hutton DL, Hung BP, Huri PY, Cook CA, Kondragunta R, Jia XF, Grayson WL. Engineering anatomically shaped vascularized bone grafts with hASCs and 3D-printed PCL scaffolds. J Biomed Mater Res, Part A. 2014; 102(12):4317–4325.
27. Yilgor P, Hasirci N, Hasirci V. Sequential BMP-2/BMP-7 delivery from polyester nanocapsules. J Biomed Mater Res, Part A. 2010; 93(2):528–36.
28. Oliveira JM, Silva SS, Malafaya PB, Rodrigues MT, Kotobuki N, Hirose M, Gomes ME, Mano JF, Ohgushi H, Reis RL. Macroporous hydroxyapatite scaffolds for bone tissue engineering applications: physicochemical characterization and assessment of rat bone marrow stromal cell viability. J Biomed Mater Res, Part A. 2009; 91(1):175–86.
29. Azami M, Samadikuchaksaraei A, Poursamar SA. Synthesis and characterization of a laminated hydroxyapatite/gelatin nanocomposite scaffold with controlled pore structure for bone tissue engineering. Int J Artif Organs. 2010; 33(2):86–95. [PubMed: 20306435]
30. Umeda H, Kanemaru S, Yamashita M, Kishimoto M, Tamura Y, Nakamura T, Omori K, Hirano S, Ito J. Bone regeneration of canine skull using bone marrow-derived stromal cells and beta-tricalcium phosphate. Laryngoscope. 2007; 117(6):997–1003. [PubMed: 17460579]
31. Nienhuijs MEL, Walboomers XF, Briest A, Merkx MAW, Stoelinga PJW, Jansen JA. Healing of bone defects in the goat mandible, using COLLOSS (R) E and beta-tricalciumphosphate. J Biomed Mater Res, Part B. 2010; 92B(2):517–524.
32. Baas J, Elmengaard B, Bechtold J, Chen X, Soballe K. Ceramic bone graft substitute with equine bone protein extract is comparable to allograft in terms of implant fixation: a study in dogs. Acta Orthopaedica. 2008; 79(6):841–50. [PubMed: 19085504]
33. Correia C, Grayson WL, Park M, Hutton D, Zhou B, Guo XE, Niklason L, Sousa RA, Reis RL, Vunjak-Novakovic G. In vitro model of vascularized bone: synergizing vascular development and osteogenesis. PLoS One. 2011; 6(12):e28352. [PubMed: 22164277]
34. Sathyavathi R, Saha A, Soares JS, Spegazzini N, McGee S, Rao Dasari R, Fitzmaurice M, Barman I. Raman spectroscopic sensing of carbonate intercalation in breast microcalcifications at stereotactic biopsy. Sci Rep. 2015; 5:9907. [PubMed: 25927331]
35. Hung BP, Babalola OM, Bonassar LJ. Quantitative characterization of mesenchymal stem cell adhesion to the articular cartilage surface. J Biomed Mater Res, Part A. 2013; 101(12):3592–8.
36. Reyes CD, Garcia AJ. A centrifugation cell adhesion assay for high-throughput screening of biomaterial surfaces. J Biomed Mater Res, Part A. 2003; 67(1):328–33.
37. Sauermann W, Feuerstein TJ. Some mathematical models for concentration-response relationships. Biom J. 1998; 40(7):865–881.
38. Feuerstein TJ, Limberger N. Mathematical analysis of the control of neurotransmitter release by presynaptic receptors as a supplement to experimental data. Naunyn-Schmiedeberg's Arch Pharmacol. 1999; 359(5):345–59. [PubMed: 10498284]
39. Hung BP, Hutton DL, Kozielski KL, Bishop CJ, Naved B, Green JJ, Caplan AI, Gimble JM, Dorafshar AH, Grayson WL. Platelet-derived growth factor BB enhances osteogenesis of adipose-derived but not bone marrow-derived mesenchymal stromal/stem cells. Stem Cells. 2015; 33(9): 2773–2784. [PubMed: 26013357]
40. Estes BT, Diekman BO, Gimble JM, Guilak F. Isolation of adipose-derived stem cells and their induction to a chondrogenic phenotype. Nat Protoc. 2010; 5(7):1294–1311. [PubMed: 20595958]
41. Hutton DL, Kondragunta R, Moore EM, Hung BP, Jia X, Grayson WL. Tumor Necrosis Factor improves vascularization in osteogenic grafts engineered with human adipose-derived stem/stromal cells. PLoS One. 2014; 9(9):e107199. [PubMed: 25248109]
42. Cowan CM, Shi YY, Aalami OO, Chou YF, Mari C, Thomas R, Quarto N, Contag CH, Wu B, Longaker MT. Adipose-derived adult stromal cells heal critical-size mouse calvarial defects. Nat Biotechnol. 2004; 22(5):560–7. [PubMed: 15077117]
43. Gupta DM, Kwan MD, Slater BJ, Wan DC, Longaker MT. Applications of an athymic nude mouse model of nonhealing critical-sized calvarial defects. J Craniofac Surg. 2008; 19(1):192–7. [PubMed: 18216688]
44. Mandair GS, Morris MD. Contributions of Raman spectroscopy to the understanding of bone strength. BoneKEy Rep. 2015; 4:620. [PubMed: 25628882]

45. Taddei P, Tinti A, Reggiani M, Fagnano C. In vitro mineralization of bioresorbable poly(epsilon-caprolactone)/apatite composites for bone tissue engineering: a vibrational and thermal investigation. J Mol Struct. 2005; 744:135–143.
46. Kister G, Cassanas G, Bergounhon M, Hoarau D, Vert M. Structural characterization and hydrolytic degradation of solid copolymers of D,L-lactide-co-epsilon-caprolactone by Raman spectroscopy. Polymer. 2000; 41(3):925–932.
47. Dalby MJ, Gadegaard N, Tare R, Andar A, Riehle MO, Herzyk P, Wilkinson CD, Oreffo RO. The control of human mesenchymal cell differentiation using nanoscale symmetry and disorder. Nat Mater. 2007; 6(12):997–1003. [PubMed: 17891143]
48. McNamara LE, McMurray RJ, Biggs MJ, Kantawong F, Oreffo RO, Dalby MJ. Nanotopographical control of stem cell differentiation. J Tissue Eng. 2010; 2010:120623. [PubMed: 21350640]
49. Hung BP, Hutton DL, Grayson WL. Mechanical control of tissue-engineered bone. Stem Cell Res Ther. 2013; 4(1):10. [PubMed: 23369796]
50. Ang KC, Leong KF, Chua CK, Chandrasekaran M. Compressive properties and degradability of poly(epsilon-caprolactone)/hydroxyapatite composites under accelerated hydrolytic degradation. J Biomed Mater Res, Part A. 2007; 80(3):655–60.
51. Goldstein SA. The mechanical properties of trabecular bone: dependence on anatomic location and function. J Biomech. 1987; 20(11–12):1055–61. [PubMed: 3323197]
52. Zein I, Hutmacher DW, Tan KC, Teoh SH. Fused deposition modeling of novel scaffold architectures for tissue engineering applications. Biomaterials. 2002; 23(4):1169–85. [PubMed: 11791921]
53. Zhou YF, Hutmacher DW, Varawan SL, Lim TM. In vitro bone engineering based on polycaprolactone and polycaprolactone-tricalcium phosphate composites. Polym Int. 2007; 56(3): 333–342.
54. Inzana JA, Olvera D, Fuller SM, Kelly JP, Graeve OA, Schwarz EM, Kates SL, Awad HA. 3D printing of composite calcium phosphate and collagen scaffolds for bone regeneration. Biomaterials. 2014; 35(13):4026–34. [PubMed: 24529628]
55. Deligianni DD, Katsala ND, Koutsoukos PG, Missirlis YF. Effect of surface roughness of hydroxyapatite on human bone marrow cell adhesion, proliferation, differentiation and detachment strength. Biomaterials. 2001; 22(1):87–96. [PubMed: 11085388]
56. Sawyer AA, Song SJ, Susanto E, Chuan P, Lam CXF, Woodruff MA, Hutmacher DW, Cool SM. The stimulation of healing within a rat calvarial defect by mPCL-TCP/collagen scaffolds loaded with rhBMP-2. Biomaterials. 2009; 30(13):2479–2488. [PubMed: 19162318]
57. Wang YK, Yu X, Cohen DM, Wozniak MA, Yang MT, Gao L, Eyckmans J, Chen CS. Bone morphogenetic protein-2-induced signaling and osteogenesis is regulated by cell shape, RhoA/ROCK, and cytoskeletal tension. Stem Cells Dev. 2012; 21(7):1176–1186. [PubMed: 21967638]
58. Bhumiratana S, Grayson WL, Castaneda A, Rockwood DN, Gil ES, Kaplan DL, Vunjak-Novakovic G. Nucleation and growth of mineralized bone matrix on silk-hydroxyapatite composite scaffolds. Biomaterials. 2011; 32(11):2812–20. [PubMed: 21262535]
59. Stoppato M, Carletti E, Sidarovich V, Quattrone A, Unger RE, Kirkpatrick CJ, Migliaresi C, Motta A. Influence of scaffold pore size on collagen I development: A new in vitro evaluation perspective. J Bioact Compat Polym. 2013; 28(1):16–32.
60. Suwanprateeb J, Sanngam R, Suvannapruk W, Panyathanmaporn T. Mechanical and in vitro performance of apatite-wollastonite glass ceramic reinforced hydroxyapatite composite fabricated by 3D-printing. J Mater Sci: Mater Med. 2009; 20(6):1281–1289. [PubMed: 19225870]

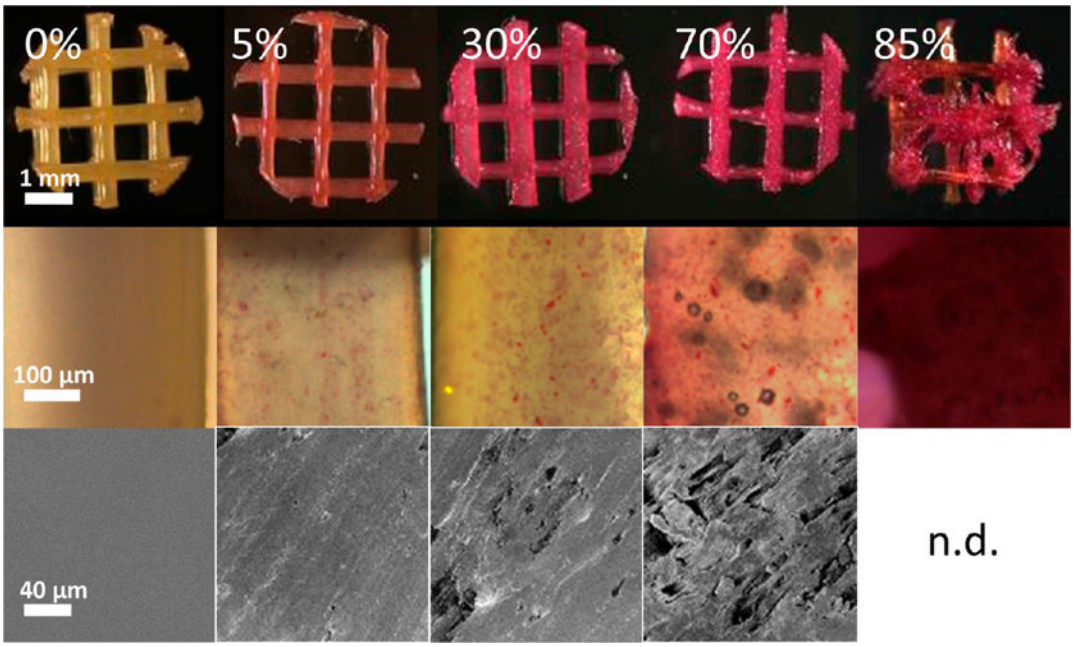

Figure 1.

Imaging of 3D-printed hybrid scaffolds. Top: Scaffolds stained positively for Alizarin Red S in all cases except for the pure polycaprolactone case. Middle: Magnified images of stained scaffold struts delineating the punctate stain of the mineralized particles within the PCL. Bottom: Scanning electron microscopy of strut surfaces revealing rougher surface topographies in the more concentrated hybrid scaffolds.

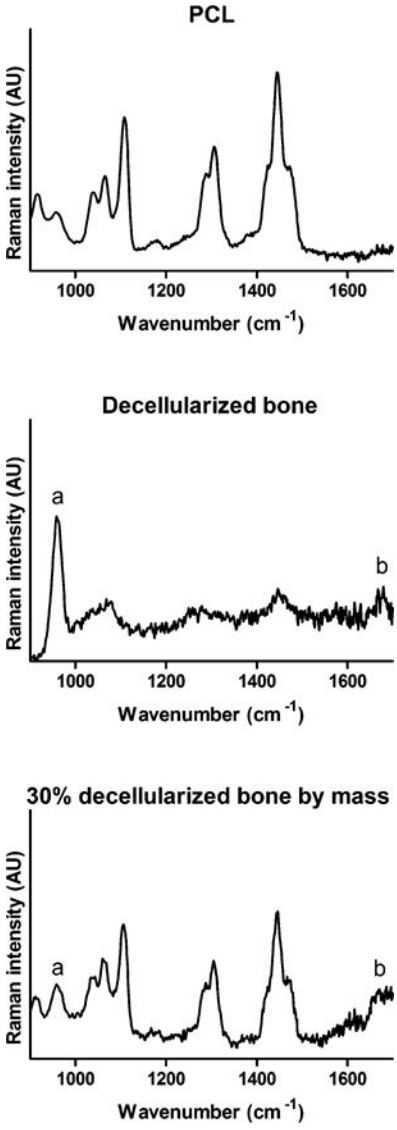

Figure 2.

Raman spectroscopy of pure and hybrid materials. Top: Raman spectra of pure polycaprolactone, revealing peaks at 1450 cm^{-1} for δCH_2, 1300 cm^{-1} for ωCH_2, and 1110 cm^{-1} for skeletal stretching. Middle: Raman spectra of decellularized trabecular bone, showing peaks at 960 cm^{-1} for phosphate (a) and 1650 cm^{-1} for collagen amide I (b). Bottom: Raman spectra of 30% DCB:PCL. The bone-only peaks as well as the peaks corresponding to contributions from both bone and polycaprolactone appear.

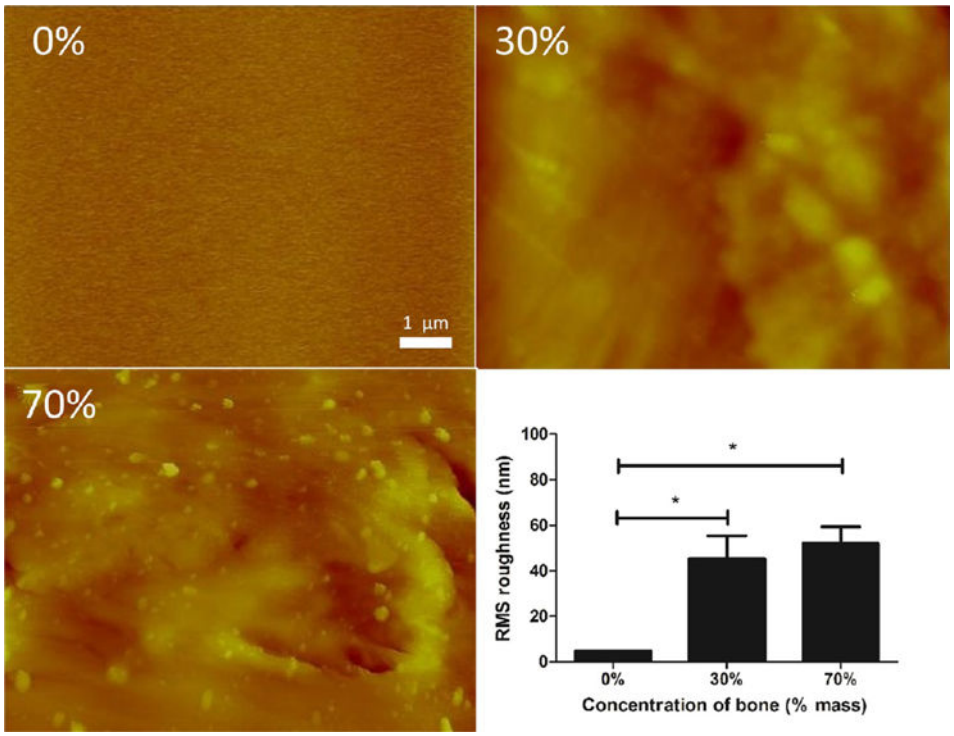

Figure 3.

Atomic force microscopy of pure and hybrid materials. Top left: Atomic force micrograph of pure polycaprolactone is mostly featureless, whereas surface features are rougher for 30% bone by mass (top right) and 70% bone by mass (bottom left). Quantification of root-mean-square roughness (bottom right) confirms these observations. $*p < 0.05$ by one-way ANOVA with posthoc Tukey test.

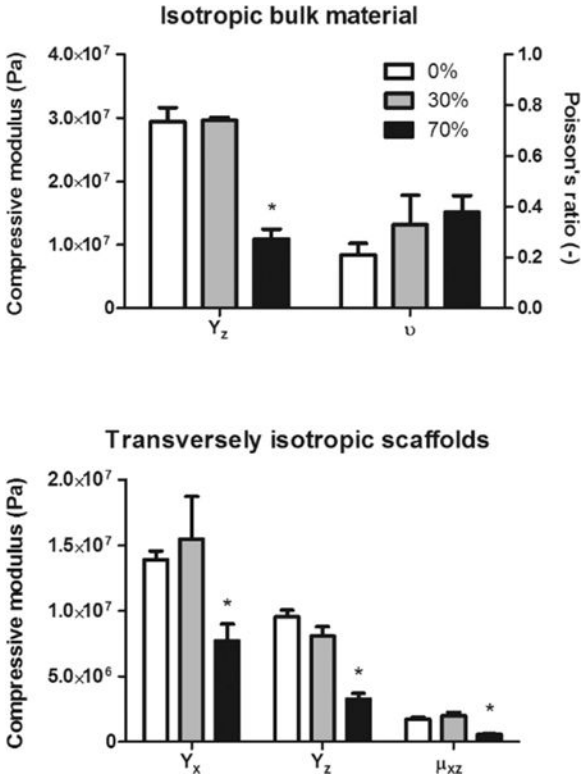

Figure 4.

Mechanical testing of pure and hybrid material/scaffolds. Top: The Poisson's ratios of all groups were not significantly different from each other, whereas the compressive modulus was significantly lower in the 70% group compared to that in both the 30% and pure groups. Bottom: The same trend held for all directions in transversely isotropic porous scaffolds. *$p < 0.05$ compared to pure polycaprolactone by one-way ANOVA with posthoc Tukey test.

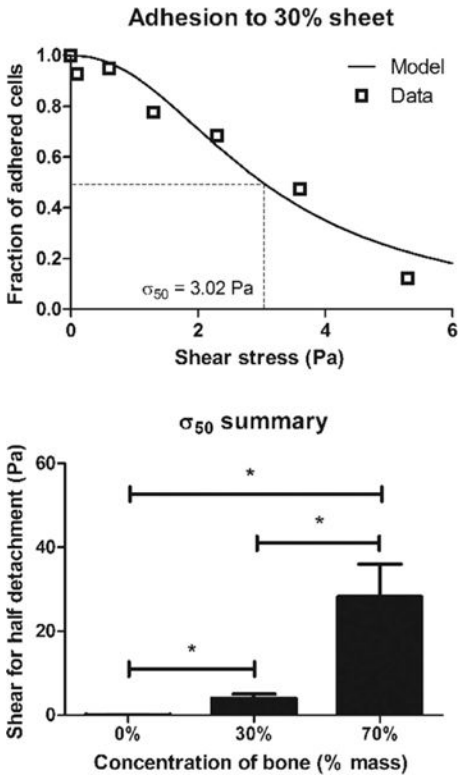

Figure 5.

Cell adhesion to pure and hybrid materials. Top: Representative graph of adhered cells plotted against shear with a variable-slope concentration response model fit to determine the shear for half-detachment, σ_{50}. Bottom: σ_{50} increases in a dose-dependent manner with increasing bone concentration. $*p < 0.05$ by one-way ANOVA with posthoc Tukey test.

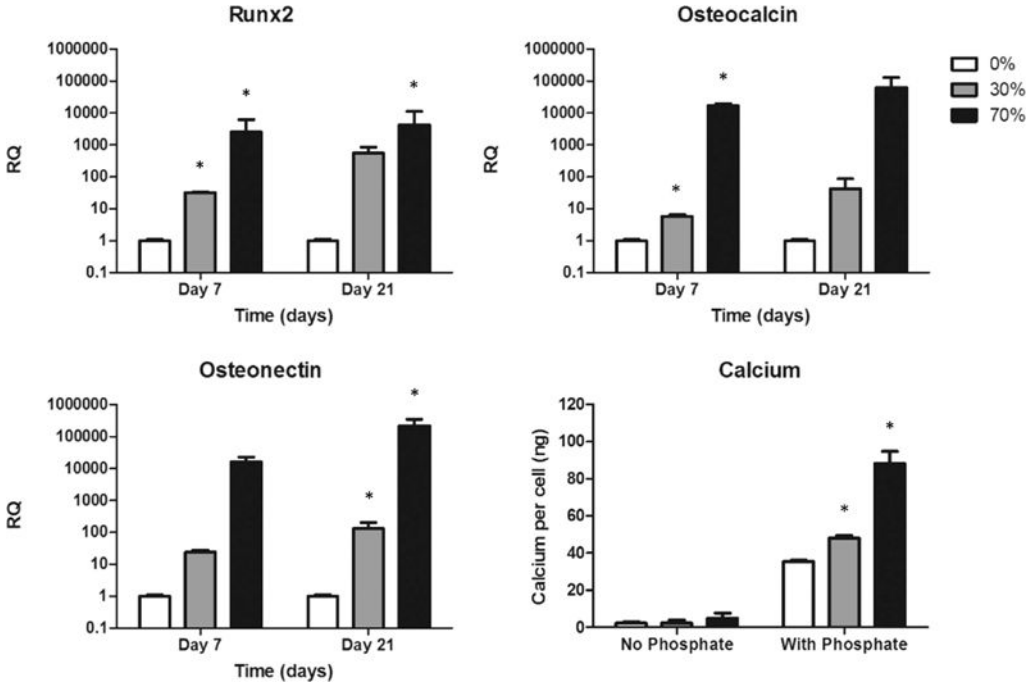

Figure 6.

In vitro osteogenic gene expression. Gene expression of Runx2, osteocalcin, and osteonectin increased in cells cultured in hybrid scaffolds despite the absence of exogenous osteoinductive factors. Bottom right: With the addition of a phosphate source, calcium production per cell displayed the same trend. $*p < 0.05$ compared to cells cultured in pure polycaprolactone scaffolds by one-way ANOVA with posthoc Tukey test.

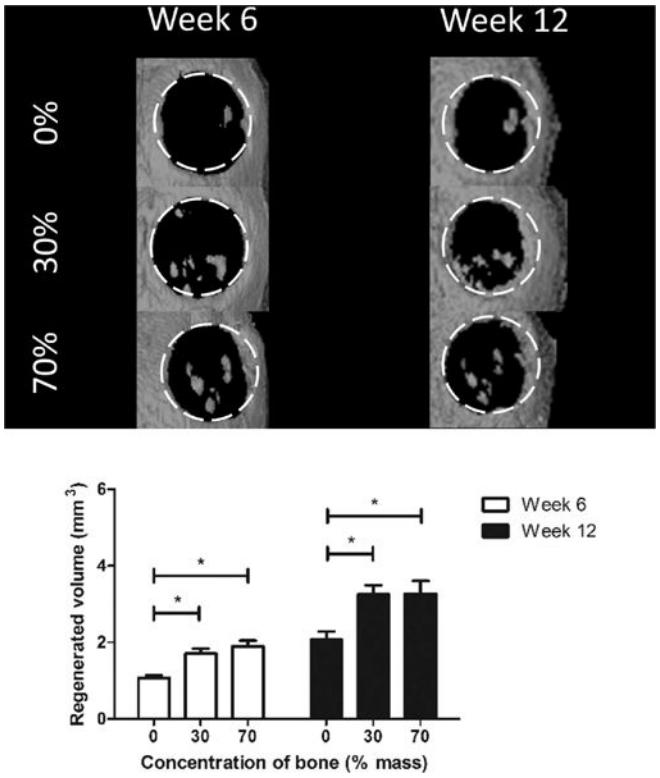

Figure 7.

In vivo regeneration of murine calvarial defect. White dotted lines show boundaries of the original defect. Top: Computed tomography scans at 6 and 12 weeks revealed increased bone regeneration in hybrid scaffold groups compared to that in the pure polycaprolactone group. Bottom: Quantification of computed tomography scans shows a significant difference between hybrid and pure PCL groups but no significant difference between the 30 and 70% groups.

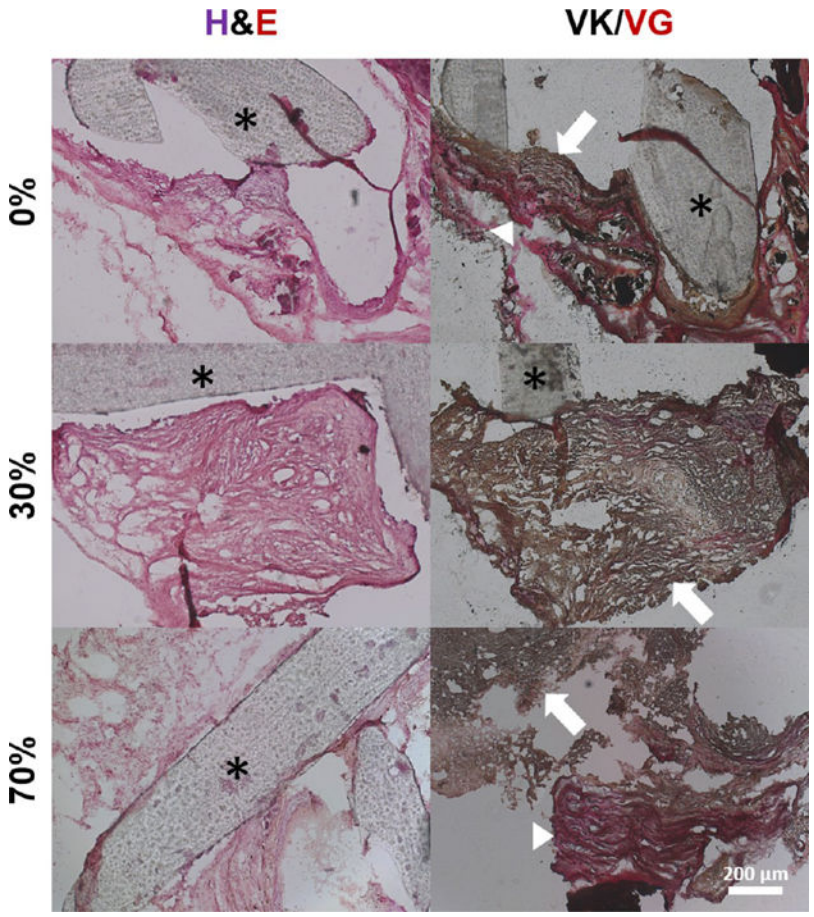

Figure 8.

Histological analysis of excised constructs. Cellularity under hematoxylin and eosin staining (left) as well as bone (black/dark brown) and osteoid (red) formation under the von Kossa and van Gieson stains (right) is evident. Asterisks denote scaffold struts. In the von Kossa and van Gieson stains, note the presence of both osteoid (red, arrowheads) and mineralized tissue (red/brown, arrows), suggesting active mineralization occurring within the constructs.

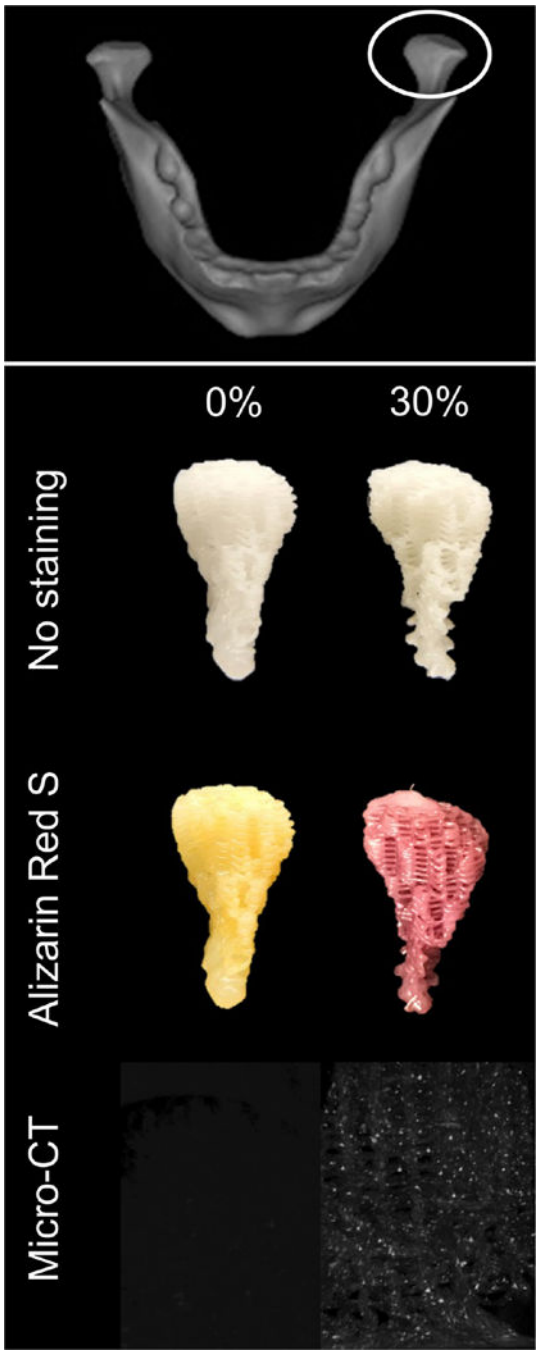

Figure 9.

Top: Anatomical shape printing of pure and hybrid scaffolds. Middle: A human temporomandibular joint condyle was isolated and printed into anatomically shaped, porous scaffolds. Scaffolds were subject to Alizarin Red S staining to confirm and visualize the presence of mineralized particles in the hybrid scaffold. Bottom: MicroCT scans performed to confirm the presence of mineralized particles in the 30% DCB:PCL scaffolds. There were no mineral particles in the pure PCL scaffold.

Table 1

concentration of bone (% mass)	print quality (−)
0	88.2
5	89.6
30	85.8
70	77.6
85	50.0